Acta Cryst. (1980). A**36**, 1–7

Short-Range Order in Ni_3Fe

BY S. LEFEBVRE, F. BLEY, M. BESSIERE AND M. FAYARD

CECM, 15, rue G. Urbain, 94400 Vitry/Seine, France

M. ROTH

Institut Laue–Langevin, BP 156 Centre de Tri, 38042 Grenoble Cedex, France

AND J. B. COHEN

Department of Materials Science and Engineering, The Technological Institute, Northwestern University, Evanston, Illinois 60201, USA

(*Received* 23 *February* 1979; *accepted* 16 *July* 1979)

Abstract

Short-range order parameters were obtained for a single crystal of $^{62}Ni_3Fe$ quenched from above T_c. These are the first absolute measurements of diffuse elastic neutron scattering complete enough to separate the effects of local order and atomic displacements (up to quadratic terms) and indicate that neutrons are ideally suited for such studies. The results are compared to those obtained with X-rays. The short-range order intensity of Ni_3Fe is similar in shape to that for Cu_3Au but in this alloy it is due to the plate-like nature of ordered domains, not the antiphase domain boundaries which are present in such regions in Cu_3Au.

I. Introduction

Since the investigations by Sykes & Jones (1937), considerable attention has been paid to ordering in the iron–nickel system, especially near the permalloy composition, Ni_3Fe (Josso, 1949; Wakelin & Yates, 1953; Drijver & Woude, 1977; Kollie & Brooks, 1973).

Above the critical temperature the degree of short-range order (SRO) appears to vary with temperature. Because of the low rate of diffusion in this system, a particular state of SRO can be conserved by quenching. Therefore, many physical properties have been shown to vary with quench temperature (Calvayrac & Fayard, 1972; Calvayrac, 1972; Calvayrac & Fayard, 1973): (i) the cell parameter, measured at room temperature, decreases with SRO; (ii) the yield stress increases; (iii) the density of states at the Fermi level, $N(E_F)$, decreases from the disordered to the long-range ordered (LRO) state (Kollie, Scarbrough & McElroy, 1970). Recent measurements (Calvayrac, 1979) show that $N(E_F)$ also decreases when SRO increases between 973 K and the critical temperature (~773 K). This diminution is 20% of the total difference between the long-range and short-range ordered states.

Thus, it is of interest to have quantitative information on the local atomic arrangement above T_c and this paper provides the results of measurements of the Cowley–Warren SRO parameters (α_l).

Because of the similarity of the scattering factors of iron and nickel, X-ray determinations of long-range or short-range order are difficult and for the latter only incomplete results have been published (Wilson & Gould, 1972). The neutron diffuse intensity scattered by natural iron–nickel alloys is similar in magnitude to X-ray scattering, but it is possible to use enriched isotopes in order to increase the difference in the scattering lengths of the nuclei. Several attempts have been made by Collins, Jones & Lowde (1962) using the ^{60}Ni isotope but the results (on powdered specimens of Ni_2Fe_3 and Ni_7Fe_3) are only qualitative. More recently, Goman'kov (1976) has performed similar measurements with powders of $^{62}Ni_3Fe$ and reports a slow variation of SRO with temperature which seems to disagree with the more rapid variation of physical properties. Moreover, an analysis of the Mössbauer spectra of Ni_3Fe alloys by Heilmann & Zinn (1967) also suggests a more rapid decrease of the local order with temperature.

In order to obtain a better idea of the structural state of this alloy we have performed an analysis of the absolute neutron diffuse intensity scattered from a $^{62}Ni_3Fe$ single crystal in a volume in reciprocal space. The results of these measurements are compared with our (previously unpublished) measurements of X-ray diffuse intensity. It is the purpose of this paper to test this method and to examine the local atomic arrangements at one temperature. Variations in the local atomic arrangements with temperature will be reported in another publication.

0567-7394/80/010001-07$01.00

II. Experimental procedures

A. Samples

For neutron measurements a cylindrically shaped crystal, 5 mm long and 5 mm thick, was grown by the Bridgman technique in an alumina crucible in argon and 5% H_2. Its axis is close to a ⟨123⟩ direction.

The isotope ^{62}Ni was employed; its composition (provided by the Russian producer) and the corresponding scattering lengths (Bacon, 1975) are given in Table 1. The chemical composition of the crystal is $Ni_{0.765}Fe_{0.235}$; it was sealed in vycor in vacuum, held for one hour at 808 K, and quenched.

Table 1. *Isotope composition and scattering lengths*

Ni isotope	62	58	60	61	64
%	97·7	1·17	0·8	0·19	0·14
b	−0·87	1·44	0·28	0·74	−0·037

The crystal used for the X-ray measurements was cut by spark machining with a surface parallel to a {112} plane from a crystal grown by the Czochralski method. The chosen composition, $Ni_{0.74}Fe_{0.26}$, corresponds to the maximum in the critical temperature *vs* iron concentration (Calvayrac & Fayard, 1972); the specimen was quenched from 793 K.

B. Measurements of neutron scattering

Neutron diffuse intensity was measured on the four-circle D10 diffractometer at the high-flux reactor of the Laue–Langevin Institute in Grenoble, France. The beam of monochromatic neutrons ($\lambda = 1{\cdot}2622$ Å) was focused vertically on the sample by a copper crystal. The divergence of the beam was measured by the width at half height of Bragg reflections; the elementary volume measured in reciprocal space at each point was between 0·01 and 0·03a^*. This resolution is much smaller than the measurement increments $\Delta h = 0{\cdot}1a^*$.

Slits to eliminate parasitic scattering coming from the cryostat walls were placed before and after the sample. The measurements were carried out at 77 K and the elastic diffuse intensity was measured with a ^3He counter placed after a graphite crystal analyzer.

With an Al crystal, the peak at the 100 position due to neutrons with wavelength $\lambda/2$ was a very narrow signal, which was easy to eliminate by a slight tilt of the crystal. The direct beam's intensity was deduced from the value of the diffuse intensity from a hollow cylinder of vanadium whose external dimensions were the same as those of the Ni_3Fe crystal.

C. Measurements of X-ray scattering

Measurements were made at Northwestern University. The device and methods of measurement conditions are fully described elsewhere (Schwartz, Morrison & Cohen, 1963; Gragg & Cohen, 1971). Cobalt $K\alpha$ radiation was employed, monochromated with a pyrolytic graphite crystal doubly bent to focus at the receiving slits. To eliminate the $\lambda/2$ component and fluorescence a pulse-height analyzer and balanced filters of Fe_2O_3 and MnO were employed. To hold counting precision to within statistical error for the time of measurement (which was two months) a monitor counter was used to measure the fluorescence from a film containing powdered V_2O_5 placed in the direct beam between monochromator and crystal. The intensity of the direct beam was deduced from the intensity of the diffraction lines of powdered aluminium (Bardhan & Cohen, 1976). The measurements were made at room temperature, with the crystal held in a primary vacuum under an attachment with a thin Be hemispherical cover.

III. Data analysis

A. Theory

The method of analysis is that of Borie & Sparks (1971) as developed by Gragg & Cohen (1971). The total diffuse intensity may be separated into terms depending on the local atomic order (I_{SRO}) and terms depending on average displacements (Q_x) and mean-square displacements (R_x and S_{xy}).

The total diffuse intensity (I_D) at a point $h_1 h_2 h_3$ in reciprocal space is a modulation of the Laue diffuse intensity and can be written

$$\begin{aligned} I_D(h_1,h_2,h_3)/N &= [I_{\text{total}}(h_1,h_2,h_3) - I_{\text{Bragg}}(h_1,h_2,h_3)]/I_{\text{Laue}} \\ &= I_{\text{SRO}}(h_1,h_2,h_3) + h_1 Q_x(h_1,h_2,h_3) \\ &\quad + h_2 Q_x(h_2,h_3,h_1) + h_3 Q_x(h_3,h_1,h_2) \\ &\quad + h_1^2 R_x(h_1,h_2,h_3) + h_2^2 R_x(h_2,h_3,h_1) \\ &\quad + h_3^2 R_x(h_3,h_1,h_2) + h_1 h_2 S_{xy}(h_1,h_2,h_3) \\ &\quad + h_2 h_3 S_{xy}(h_2,h_3,h_1) + h_3 h_1 S_{xy}(h_3,h_1,h_2), \end{aligned} \quad (1)$$

with

$$I_{\text{SRO}}(h_1,h_2,h_3) = \sum_l \sum_m \sum_n \alpha_{lmn} \cos \pi l h_1 \cos \pi m h_2 \times \cos \pi n h_3, \quad (2a)$$

$$Q_x(h_1,h_2,h_3) = \sum_l \sum_m \sum_n \gamma^x_{lmn} \sin \pi l h_1 \cos \pi m h_2 \cos \pi n h_3, \quad (2b)$$

$$R_x(h_1,h_2,h_3) = \sum_l \sum_m \sum_n \delta^x_{lmn} \cos \pi l h_1 \cos \pi m h_2 \cos \pi n h_3, \quad (2c)$$

$$S_{xy}(h_1,h_2,h_3) = \sum_l \sum_m \sum_n \varepsilon^{xy}_{lmn} \sin \pi l h_1 \sin \pi m h_2 \cos \pi n h_3, \quad (2d)$$

$$\gamma^{x}_{lmn} = 2\pi\{[f_A/(f_A - f_B)](C_A/C_B + \alpha_{lmn})\langle x^{AA}_{lmn}\rangle - [f_B/(f_A - f_B)](C_B/C_A + \alpha_{lmn})\langle x^{BB}_{lmn}\rangle\}, \quad (3a)$$

$$\delta^{x}_{lmn} = -2\pi^2\{[f_A^2/(f_A - f_B)^2]\langle (x^{AA}_{lmn})^2\rangle + [f_B^2/(f_A - f_B)^2]\langle (x^{BB}_{lmn})^2\rangle + [2f_A f_B/(f_A - f_B)^2]\langle (x^{AB}_{lmn})^2\rangle\}, \quad (3b)$$

$$\varepsilon^{xy}_{lmn} = -4\pi^2\{[f_A^2/(f_A - f_B)^2]\langle (xy)^{AA}_{lmn}\rangle + [f_B^2/(f_A - f_B)^2]\langle (xy)^{BB}_{lmn}\rangle + [2f_A f_B/(f_A - f_B)^2]\langle (xy)^{AB}_{lmn}\rangle\}, \quad (3c)$$

where l, m, n take integral values and specify an interatomic vector; α_{lmn} is the Cowley–Warren parameter (Cowley, 1950) $= 1 - P^{AB}_{lmn}/C_B$ where P^{AB}_{lmn} is the conditional probability of finding a B atom at site lmn relative to an A atom, and the atomic fraction of B is C_B. The coefficient γ^{xx}_{lmn} is a function of the average variation of the x component of the distance between each pare of atoms, and φ^{xx}_{lmn} and ε^{xy}_{lmn} are related to the variance of such distances, as can be seen in (3*a*)–(3*c*). The scattering factors f_i include a Debye–Waller factor (see below).

The volume to be sampled and the procedures for separating the different components of the intensity (I_{SRO}, Q_x, R_x, S_{xy}) which have different symmetries in reciprocal space, have been described by both Borie & Sparks (1971) and Gragg & Cohen (1971). In the separation methods and Fourier inversions of the different intensity components due to displacement it is necessary to assume that the coefficients γ, δ, ε are constant in reciprocal space. However, as can be seen in (3*a*) to (3*c*) there are scattering factor ratios in the displacement terms. Over the volume measured here with X-rays, these vary from ~30 to ~12.

B. Laue intensity

For X-ray diffuse scattering, the Laue scattering is

$$C_A C_B[f_A \exp(-W_A) - f_B \exp(-W_B)]^2, \quad (4)$$

where $W = B(\sin\theta/\lambda)^2$, the Debye–Waller factor.

For the alloys studied here with X-rays, the Laue monotonic scattering is very weak. It depends mainly on the dispersion correction and its value varies from ~4 to ~2 between the limits of measurement, $\sin\theta/\lambda =$ 0·14 to 0·51. The scattering factors were taken from Doyle & Turner (1968) and the dispersion corrections from Cooper (1963).

The Debye–Waller factor was measured at room temperature by Calvayrac (1972) on disordered Ni_3Fe: $B_{\mathrm{Ni}} = 0{\cdot}4 = B_{\mathrm{Fe}}$. From these the value at 77 K needed for the neutron study were calculated to be $B_{\mathrm{Fe}} = B_{\mathrm{Ni}} =$ 0·172.

For the case of unpolarized neutron scattering by the demagnetized sample of Ni_3Fe, the Laue monotonic scattering is the sum of the nuclear and the magnetic terms:

$$I^{\mathrm{I}}_{\mathrm{Laue}} = C_A C_B[b_A \exp(-W_A) - b_B \exp(-W_B)]^2, \quad (5a)$$

$$I^{\mathrm{II}}_{\mathrm{Laue}} = \tfrac{2}{3}C_A C_B[P_A \exp(-W_A) - P_B \exp(-W_B)]^2. \quad (5b)$$

Here, b_A and b_B are the coherent nuclear scattering lengths and P_A and P_B are the magnetic scattering lengths which are proportional to the magnetic moment, μ, at each atom and the magnetic form factor, f:

$$P = 0{\cdot}27\ \mu f \times 10^{-11}\ \mathrm{mm}. \quad (6)$$

According to Shull & Wilkinson (1955), $\mu_{\mathrm{Fe}} = 2{\cdot}97$ and $\mu_{\mathrm{Ni}} = 0{\cdot}62$ BM. The magnetic form factors were taken from Bacon (1975).

As is shown in Fig. 1, the magnetic contribution is weak in comparison to the nuclear contribution.

C. Corrections to the measured intensity

In the measurements with neutrons, the analyzer essentially eliminates the inelastic component and measurements may be made close to Bragg peaks. As

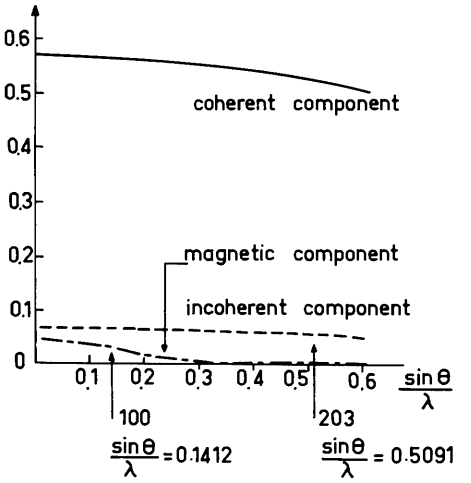

Fig. 1. Intensity of the different Laue terms and the incoherent scattering for the neutron study.

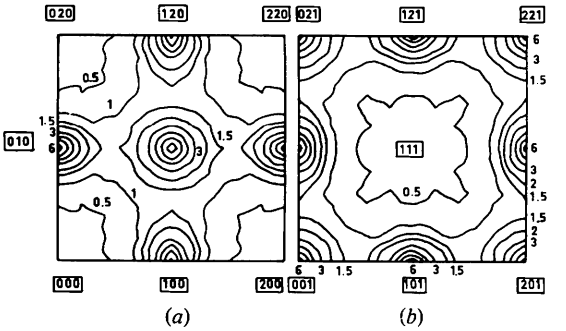

Fig. 2. Experimental intensity (*a*) $h_3 = 0$, (*b*) $h_3 = 1$.

the nuclear moments of isotopes of natural iron and of ^{62}Ni are zero there is no spin incoherency in the alloy. The diffuse incoherent intensity, due to the mixture of nuclei, is ~12% of the Laue scattering (see Fig. 1).

In comparison, in the case of X-ray scattering, the Laue diffuse intensity is so weak that all corrections – Compton (*International Tables for X-ray Crystallography*, 1962), polarization, *etc.* – are quite important. The TDS was calculated following Walker & Chipman (1970) with the elastic constants measured by Turchi, Calvayrac & Plicque (1978). This intensity was subtracted from the total X-ray intensity prior to analysis, to attempt to reduce the effect of the variation of the scattering factors in the separation by reducing the contribution of the displacement terms.

After corrections for polarization and background,

Table 2. *Results of the Fourier and least-squares analyses of the neutron data*

			Fourier analysis				
i	*lmn*	Ordered state	Full volume	Volume for SRO only	6% decrease in scale factor full volume	Least-squares analysis without displacement terms	4,000 atom simulation (* were employed to make the simulation)
0	000	1	0·946	0·964	1·01	1	
1	110	−1/3	−0·110	−0·109	−0·117	−0·12	*
2	200	+1	0·138	0·137	0·147	0·15	*
3	211	−1/3	−0·0104	−0·0115	−0·0111	−0·013	*
4	220	+1	0·055	0·054	0·0585	0·055	0·0530
5	310	−	−0·0247	−0·0239	−0·0262	−0·025	−0·0225
6	222	+	0·0331	0·0325	0·0353	0·038	*
7	321	−	−0·0113	−0·0118	−0·012	−0·013	−0·0119
8	400	+	0·0328	0·0291	0·0349	0·034	0·0344
9	411	−	0·0004	−0·0003	0·000464	0·0006	−0·0047
	330	−	−0·006	−0·00577	−0·00638	−0·0093	−0·0003
10	420	+	0·0216	0·0188	0·0230	0·023	0·0217
11	332	−	−0·0067	−0·00496	−0·00717	−0·0019	*
12	422	+	0·0135	0·0133	0·0144	0·02	0·0092
13	510	−	−0·010	−0·00682	−0·0107	−0·011	−0·0021
	431	−	−0·00186	−0·00178	0·0197	−0·0036	−0·0022
14	521	−	−0·0044	−0·00461	−0·00462	−0·0065	*
15	440	+	0·0065	0·00539	0·00695	0·0054	0·0113
16	530	−	−0·0014	−0·00356	−0·00151	−0·0042	−0·0086
	433	−	−0·0006	−0·00192	−0·000687	−0·0029	−0·0061
17	600	+	0·00698	0·00650	0·00747	0·013	0·0043
	442	+	0·00443	0·00493	0·00473	0·0014	0·0005
18	611	−	0·00305	0·00138	0·00324		0·0054
	532	−	−0·00267	−0·0027	−0·00273		0·0029
19	620	+	0·00345	0·00362	0·00368		−0·0053
20	541	−	−0·0023	−0·00133	−0·00248		−0·0054
21	622	+	0·00285	0·00446	0·0013		−0·0094
22	631	−	−0·00107	−0·00035	−0·00113		0·0102
23	444	+	0·0008	0·0018	0·00095		0·0036
24	550	−	−0·000685	−0·00156	−0·00076		0·0025
	543	−	−0·00178	−0·00144	−0·00185		0·0026
	710	−	−0·00275	−0·00357	−0·00294		−0·0035
25	640	+	0·00170	0·0027	0·00186		−0·0024
26	633	−	0·000595	0·00039	0·00063		−0·0038
	552	−	−0·001	0·00038	−0·00106		−0·0098
	721	−	−0·00151	−0·00195	−0·00264		0·0009
27	642	+	0·00008	0·00246	0·0027		−0·0118
28	730	−	−0·00083	−0·00071	−0·0009		−0·0083
29	732	−	0·00124	0·00053	0·00123		0·0034
	651	−	−0·00008	−0·00052	−0·00012		0·0048
30	800	+	0·0043	0·0048	0·00467		0·0062
31	741	−	−0·0019	−0·000357	−0·00197		0·0023
	554	−	−0·0013	−0·000414	−0·00134		
	811	−	−0·00075	−0·0011	−0·00074		
32	644	+	0·00033	0·00143	0·00042		
	820	+	0·003	0·00285	0·00324		−0·0067
33	653	−	0·00048	0·00012	0·005		0·0020
34	660	+	0·00298	0·00074	0·00306		
	822	+	0·00405	0·0015	0·00424		

the intensity was placed on an absolute scale; the calculated incoherent intensity (Compton in the case of X-rays and isotopic incoherency in the case of neutrons) as well as I^{II}_{Laue} was subtracted prior to the separation of the various terms in (1).

IV. Results and discussion

The neutron diffuse intensity (Fig. 2) shows maxima at the $L1_2$ superstructure positions; no other maxima were observed elsewhere in the reciprocal cell [as for example those found by Bardhan & Cohen (1976) in their study of Cu_3Au].

The values of the Cowley–Warren coefficients α_i are given in Table 2. The values of the coefficients found by Fourier inversion after the separation of the intensity due to displacements are compared to those found from the least-squares procedure developed by Williams (1972).

Values were obtained with two scale factors that represent the uncertainty in the direct beam intensity and therefore provide an estimate of the range of errors. The value of α_0 is very near unity (its theoretical value), differing only by the uncertainty of the normalization factor. There are only a very few measurements of this kind in the literature with this quality.

The intensity due to static displacements is very weak and is the same magnitude as the measurement error. Therefore, no size coefficients are reported. Also this is perhaps the explanation for the similarity of the results from the Borie & Sparks (1971) treatment and the method of Williams (1972), which rarely show such agreement unless the intensity is narrowly confined in reciprocal space, as it is in this case. Because this displacement scattering is so small, an analysis of the diffuse intensity in the first Brillouin zone, ignoring size contributions, gives the same values for the α_i, α_0 differing by only 0·2%, Table 2, column 5.

The diffuse peaks around the superstructure position do not have a spherical shape but (as in gold–copper alloys) are plate-like (Fig. 2). This shape is related to the values of α_3, α_5 and α_8 which don't follow the smooth decrease of α with distance obeyed by the other α's, as can be seen in Fig. 3. If these parameters are altered to values on the curves in Fig. 3, the diffuse intensity becomes spherical in shape near the superstructure positions.

The sign of the α values oscillates up to the 33rd shell in the same way as in the ordered phase. A large number of terms has to be included to match calculated and measured intensities near the superstructure positions, Figs. 4 and 5.

The X-ray diffuse intensity was rather difficult to analyze because of the small value of the Laue intensity which depends uniquely on the dispersion corrections. Errors were undoubtedly introduced by the large correction for TDS. Moreover, the X-ray scattering factor ratios $(f_i/\Delta f_i)^2$ vary greatly in reciprocal space as was previously mentioned.

Nevertheless, the separation of I_{SRO} from the total intensity does not seem too bad, as the values of α_1, α_2, and α_3, Table 3, are not very different from those

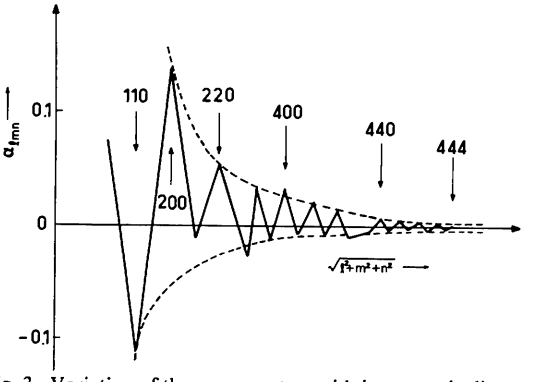

Fig. 3. Variation of the α parameters with interatomic distance.

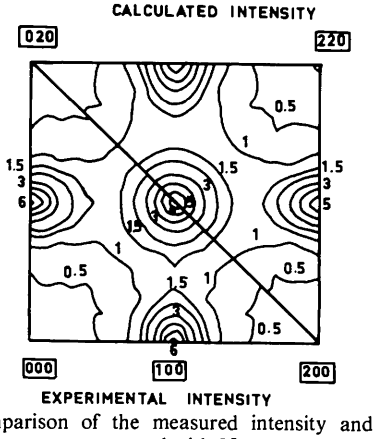

Fig. 4. Comparison of the measured intensity and that reconstructed with 33 α's.

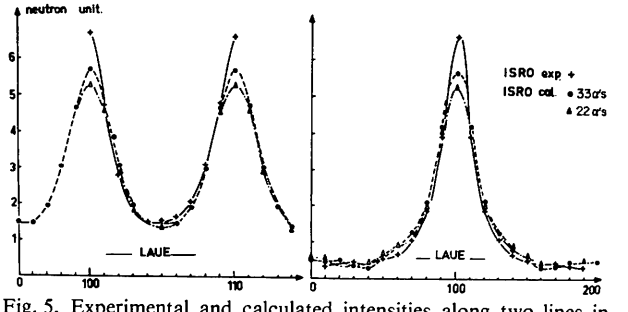

Fig. 5. Experimental and calculated intensities along two lines in reciprocal space. Bragg peak → SRO peak (000 → 100) and SRO peak → SRO peak (100 → 110).

Table 3. *Value of the α_i parameter obtained with X-rays*

α_0	α_1 110	α_2 200	α_3 211	α_4 220	α_5 310
2·1	−0·16	0·105	−0·044	−0·058	0·1

measured in the neutron experiment, Table 2. However, α_0 was 2·1, and higher-order terms differ considerably in the two measurements.

Another way to examine the success of the separation method is to consider the value of I_{SRO} at symmetry-equivalent positions. In the X-ray measurements, these vary by factors of 7–8 or more, even in regions of strong intensity, whereas for neutrons, the variation was typically 7% and occasionally as large as 17%.

These measurements clearly demonstrate that absolute neutron scattering measurements can be employed to obtain detailed information on local order and displacements, and that the Borie–Sparks procedure is quite satisfactory with neutrons, whereas it is not adequate with X-rays if the ratio $f_i/\Delta f$ varies appreciably.

Computer simulations were made with 4000 atoms and periodic boundary conditions to satisfy $\alpha_1, \alpha_2, \alpha_3, \alpha_6, \alpha_{11}, \alpha_{14}$, in column 4 of Table 2 to 1% (Gehlen & Cohen, 1965; Gragg, Bardhan & Cohen, 1971). The other α_i from the model are given in the last column of Table 2, where they can be compared to the measured values. (The model's values were similar when only α_i–α_6 were employed in the simulation.) Such simulations were of interest because the disc-like I_{SRO} is quite similar to that in Cu_3Au. For this latter alloy, this shape is thought to be due to antiphase domain boundaries on {100} planes in small ordered regions (Gehlen & Cohen, 1965). But in ordered Ni_3Fe, the domain-boundary energy is much less anisotropic than in Cu_3Au (Calvayrac & Fayard, 1965), and such boundaries might be expected to be on many planes. In fact the simulations showed that the regions in Ni_3Fe contain no such boundaries; the shapes of I_{SRO} appear to be due to the plate-like nature of the ordered regions, with {100} habit planes. Such regions, 2–3 layers thick, containing 10–20 atoms (six unit cells) are the predominant feature of the simulations, although there are some plates 4–5 layers thick and some thick rods.

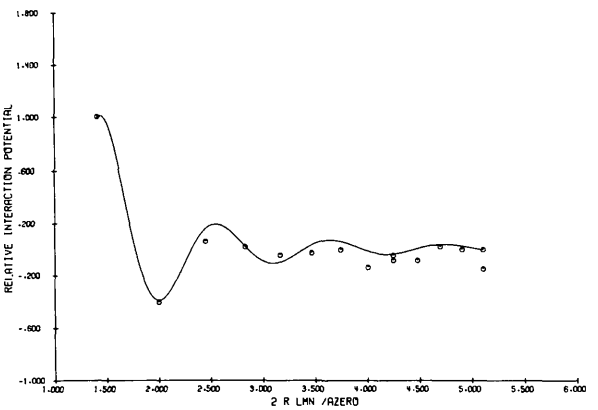

Fig. 6. Pair potentials (circles) *vs* interatomic distance (normalized by the lattice parameter, '*a* zero'). Solid line: $A = 3{\cdot}24 \cos(2{\cdot}3696 r_{lmn} - 2{\cdot}4814)/r^3_{lmn}$.

These plates are occasionally attached at corners or edges, but not on faces. A second simulation was made increasing α_3 to the value at the envelope in Fig. 3. The only effect was to increase the size of the ordered regions and make them more three dimensional, which was already indicated above by the fact that this made the scattering more symmetric. In the random simulation, all regions were less than 10 atoms in size. Thus the disc-like diffuse scattering can be thought to be due primarily to the intersection of short thick rods from the ordered plates in this alloy. The SRO is due to these plates suspended in a near-random matrix; some 1400 of the 4000 atoms were in these well-ordered regions.

Finally, in Fig. 6 we present the pair potentials derived from I_{SRO}, following the procedures described by Ohshima & Watanabe (1976). It is surprising how well these potentials fit a simple Friedel oscillatory potential (solid line), despite the fact that in transition elements the *d* band is narrow and the Fermi surface is complex in shape.

We gratefully acknowledge Dr Yvonne Calvayrac who prepared the single crystals, and for all the fruitful discussions we have had together.

We wish to thank Dr Zeyen for his help in using the D10 diffractometer at the Laue–Langevin Institute.

X-ray measurements were carried out at Northwestern University where the data analysis package was also developed; this was supported by NSF under Grant No. DMR 76-80662-A01. Portions of the work were performed in the long-term X-ray facility of the Materials Research Center, partially supported under the NSF-MRL program (Grant No. DMR 76-80847). Mr C. Tang provided valuable assistance in carrying out the simulations and determining the pair potentials.

References

BACON, G. E. (1975). *Neutron Diffraction*. Oxford: Clarendon Press.

BARDHAN, P. & COHEN, J. B. (1976). *Acta Cryst.* A**32**, 597–614.

BORIE, B. & SPARKS, C. J. (1971). *Acta Cryst.* A**27**, 198–201.

CALVAYRAC, Y. (1972). PhD Thesis, Univ. of Paris.

CALVAYRAC, Y. (1979). To be published.

CALVAYRAC, Y. & FAYARD, M. (1965). *C.R. Acad. Sci.* **260**, 6115–6117.

CALVAYRAC, Y. & FAYARD, M. (1972). *Mater. Res. Bull.* **7**, 891–902.

CALVAYRAC, Y. & FAYARD, M. (1973). *Phys. Status Solidi*, **17**, 407–421.

COLLINS, M. F., JONES, R. V. & LOWDE, R. D. (1962). *J. Phys. Soc. Jpn*, Vol. 17 supplement B III, *Proceedings of the* 1961 *International Conference on Magnetism and Crystallography*, Vol. III, pp. 19–26.

COOPER, M. J. (1963). *Acta Cryst.* **16**, 1067–1069.

COWLEY, J. M. (1950). *J. Appl. Phys.* **21**, 24–30.

DOYLE, P. A., TURNER, P. S. (1968). *Acta Cryst.* A**24**, 390–397.
DRIJVER, J. N. & WOUDE, F. (1977). *Phys. Rev.* **16**, 993–1000.
GEHLEN, P. & COHEN, J. B. (1965). *Phys. Rev.* **139**, A844–A855.
GOMAN'KOV, V. I. (1976). *Fiz. Met. Metalloved.* **42**, no. 2, 415–418.
GRAGG, J. E. JR, BARDHAN, P. & COHEN, J. B. (1971). *Critical Phenomena in Alloys, Magnets and Superconductors*, edited by R. E. MILLS, E. ASCHER & R. I. JAFFEE, pp. 309–337. New York: McGraw-Hill.
GRAGG, J. E. & COHEN, J. B. (1971). *Acta Metall.* **19**, 507–519.
HEILMANN, A. & ZINN, W. (1967). *Z. Metallkd.* **58**, 113–120.
International Tables for X-ray Crystallography (1962). Vol. III. Birmingham: Kynoch Press.
JOSSO, E. (1949). *C. R. Acad. Sci. Paris*, **229**, 594–596.
KOLLIE, T. G. & BROOKS, C. R. (1973). *Phys. Status Solidi*, **19**, 545–553.
KOLLIE, T. G., SCARBROUGH, J. O. & MCELROY, D. L. (1970). *Phys. Rev. B*, **8**, 2831–2839.
OHSHIMA, K. & WATANABE, D. (1976). *Acta Cryst.* A**32**, 883–892.
SCHWARTZ, L. H., MORRISON, L. A. & COHEN, J. B. (1963). *Adv. X-ray Anal.* **7**, 281–301.
SHULL, C. G. & WILKINSON, M. K. (1955). *Phys. Rev.* **97**, 304–310.
SYKES, C. & JONES, F. W. (1937). *Proc. R. Soc. London Ser. A*, **440**, 444.
TURCHI, P., CALVAYRAC, Y. & PLICQUE, F. (1978). *Phys. Status Solidi*, **45**, 229–238.
WAKELIN, R. J. & YATES, E. L. (1953). *Proc. Phys. Soc. London Sect. B*, **66**, 221–223.
WALKER, C. B. & CHIPMAN, D. R. (1970). *Acta Cryst.* A**26**, 447–455.
WILLIAMS, R. O. (1972). ORNL Report 5, Oak Ridge National Laboratory, Tennessee.
WILSON, W. L. & GOULD, R. (1972). *J. Appl. Cryst.* **5**, 125–127.

Acta Cryst. (1980). A**36**, 7–15

A Neutron Diffraction Study of Anharmonic Thermal Vibrations in Cubic $CsPbX_3$

BY M. SAKATA,* J. HARADA,† M. J. COOPER AND K. D. ROUSE

*Materials Physics Division, AERE, Harwell, Oxon., OX*11 0*RA, England*

(*Received* 23 *April* 1979; *accepted* 26 *July* 1979)

Abstract

A neutron diffraction study of cubic $CsPbX_3$ (X = Cl or Br) has been carried out over the temperature ranges 325–623 K for $CsPbCl_3$ and 408–673 K for $CsPbBr_3$. The temperature factors for the perovskite structure were derived following the method of Matsubara [*Prog. Theor. Phys.* (1975), **53**, 1210–1211] which includes the use of cumulant coefficients to characterize anharmonic components for an Einstein model. The potential parameters were then obtained using a numerical integration method to analyse the temperature dependence of the temperature factors. It was found that the anharmonic components in the potential were very large for the Cs and X atoms which undergo displacements on passing through the phase transitions at lower temperatures (321 K for $CsPbCl_3$ and 403 K for $CsPbBr_3$). On the other hand, a harmonic potential is quite adequate to describe the thermal vibration of the Pb atoms, which are not displaced at the phase transitions. Thus, the existence of the anharmonicity in the cubic phase seems to be anticipating the atomic displacement through the successive phase transitions for these substances. In addition to this anharmonicity, the temperature factors of the X atoms parallel to the (100) plane show an anomalous behaviour near the cubic to tetragonal phase-transition temperature, which should be connected with the softening of phonon mode at this phase transition.

1. Introduction

Cesium lead chloride, $CsPbCl_3$, and cesium lead bromide, $CsPbBr_3$, have a cubic perovskite structure at high temperature and show similar successive structural phase transitions from the viewpoint of atomic displacements through the phase transitions; that is, the first phase transition from the high-temperature side is due to the condensation of the M_3 mode, in which atomic displacement is allowed only for X (X = Cl, Br) atoms and others are due to the condensation of the Z_9‡

* On leave from Nagoya University, Nagoya, Japan.
† Applied Physics, Nagoya University, Nagoya, Japan.

‡ This notation is following the representation given by Olbrychski (1963).

0567-7394/80/010007-09$01.00